Phase equilibria in the La–Mg–Ge system at 500 °C and crystal structure of the new ternary compounds $La_{11}Mg_2Ge_7$ and $LaMg_{3-x}Ge_2$

S. De Negri[1*], P. Solokha[1], M. Skrobańska[1], D.M. Proserpio[2], A. Saccone[1]

[1]Università degli Studi di Genova, Dipartimento di Chimica e Chimica Industriale, via Dodecaneso 31, 16146 Genova, Italy

[2]Università degli Studi di Milano, Dipartimento di Chimica, Via Golgi 19, 20133 Milano, Italy and Samara Center for Theoretical Materials Science (SCTMS) Samara State University, Samara 443011, Russia

Abstract

The whole 500 °C isothermal section of the La–Mg–Ge ternary system was constructed ~~in the whole composition range~~. The existence and crystal structure of three ternary compounds were confirmed: $La_{2+x}Mg_{1-x}Ge_2$ (τ_2, *P*4/*mbm*, *tP*10–Mo_2FeB_2, $0 \le x \le 0.25$), $La_4Mg_5Ge_6$ (τ_3, *Cmc*2$_1$, *oS*60–$Gd_4Zn_5Ge_6$) and $La_4Mg_7Ge_6$ (τ_4, *C*12/*m*1, *mS*34, own structure type). Five novel compounds were identified and structurally characterized: $La_{11}Mg_2Ge_7$ (τ_1, *P*4$_2$/*ncm*, *tP*88-8, own structure type, $a = 1.21338(5)$, $c = 1.57802(6)$ nm), $LaMg_{3-x}Ge_2$ (τ_5, *P* $\bar{3}$1*c*, *hP*34-0.44, own structure type, x=0.407(5), $a = 0.78408(4)$, $c = 1.45257(7)$ nm), $La_6Mg_{23}Ge$ (τ_6, *Fm*-3*m*, *cF*120–$Zr_6Zn_{23}Si$, $a = 1.46694(6)$ nm), La_4MgGe_{10-x} (τ_7, x=0.37(1), *C*2/*m*, *mS*60-1.46, own structure type, $a = 0.88403(8)$, $b = 0.86756(8)$, $c = 1.7709(2)$ nm, $\beta = 97.16°(1)$ and La_2MgGe_6 (τ_8, *Cmce*, *oS*72–$Ce_2(Ga_{0.1}Ge_{0.9})_7$, $a = 0.8989(2)$, $b = 0.8517(2)$, $c = 2.1064(3)$ nm). Disordering phenomena were revealed in several La–Mg–Ge phases in terms of partially occupied sites. The crystal structures of $La_{11}Mg_2Ge_7$ and $LaMg_{3-x}Ge_2$ are discussed in details. The latter is a $\sqrt{3}a \times \sqrt{3}a \times 2c$ superstructure of the $LaLi_3Sb_2$ structure type; the symmetry reduction scheme is shown in the *Bärnighausen* formalism terms.

KEYWORDS. Germanides, Phase equilibria, Crystal structure, Single-crystal X-ray diffraction, Group-subgroup relation

* Corresponding author. E-mail for S.D.: serena.denegri@unige.it

1. Introduction

The R–M–Ge systems (R = rare earth metal, M = *s*- or *p*-block metal, Zn) have recently gained significant importance thanks to the existence of numerous ternary compounds, generally described as polar intermetallics, showing a variety of structural fragments based on Ge–Ge covalent interactions stabilized by the element M and balanced by the electropositive counterpart R [1-3]. These compounds provide a valuable dataset to study the interplay between composition, crystal structure and chemical bonding peculiarities of intermetallics. In this framework, we focused on the La–Mg–Ge system, with the aim to enrich the largely unexplored family of Mg-containing germanides, and thus the crystal structure and chemical bonding of $La_4Mg_5Ge_6$ and $La_4Mg_7Ge_6$ were elucidated [4]. The whole composition range of the chosen system was then searched; in this work results on phase equilibria and several new ternary La–Mg–Ge compounds are discussed.

The three binary boundary phase diagrams of the studied system are briefly commented in the following. A re-investigation of the La–Mg phase diagram [5] confirmed the existence of six intermetallic phases (LaMg, $LaMg_2$, $LaMg_3$, La_5Mg_{41}, La_2Mg_{17} and $LaMg_{12}$), all forming peritectically except for $LaMg_3$, which forms congruently. The compounds $LaMg_2$ and La_5Mg_{41} are reported not to be stable below 725 and about 600 °C respectively. The crystal structures of La_2Mg_{17} and $LaMg_{12}$ were recently re-determined [6, 7].

Only the stoichiometric compound Mg_2Ge, congruently forming at 1117 °C, exists in the Mg–Ge phase diagram [8].

In the La–Ge assessed phase diagram six intermetallic phases are included [9]: La_3Ge, La_5Ge_3, La_4Ge_3, La_5Ge_4, LaGe and $LaGe_{2-x}$. For the compounds La_3Ge and LaGe two different polymorphic modifications are reported in the literature. The orthorhombic modification of La_3Ge (*oP*16–Fe_3C, denoted as α) was determined by Garde *et al.* [10] on a powder sample annealed at 500 °C; a tetragonal modification of the same phase (*tP*32–Ti_3P, denoted as β) was proposed by Gryniv *et al.* [11] based on X-ray single crystal diffraction data and by Guloy and Corbett [12] based on X-ray powder diffraction data. The temperature range of stability of the tetragonal structure is not specified, although it is referred as the high temperature modification [8]. The LaGe compound is reported to crystallize in the *oP*8–FeB structure type by many authors, nevertheless another crystal structure, *oS*16-LaSi type, was subsequently proposed to be stable at room temperature [13].

The $LaGe_{2-x}$ phase was studied in detail by Guloy and Corbett [14], who established a homogeneity range from x=0.33 to x=0.40. Two related Ge-deficient crystal structure models were proposed for this phase, the high temperature form *tI*12-α$ThSi_2$ (β$LaGe_{2-x}$) and the low temperature form *oI*12–α$GdSi_2$

($\alpha LaGe_{2-x}$). According to [14] the orthorhombic structure transforms, on heating, into the tetragonal one by means of a second-order transition occurring in the temperature range 425-635 °C with decreasing *x*. The transition was observed by high-temperature X-ray diffraction; no tetragonal phase was found by these authors at room temperature, even after quenching. Subsequently some other ordered $ThSi_2$-type derivatives were proposed to exist in the compositional region 60-65 at% Ge [15], but no complete structural data were provided. A recent work by Zhang et al. [16] shed more light on the crystal structures of the RGe_{2-x} germanides ($0.5<x<0$; R = light rare earth metal). In fact, most of these compounds show partial or total Ge vacancies ordering, which gives origin to many different superstructures depending both on composition and method of synthesis, and often difficult to fully characterize by the standard X-ray techniques. Some of such superstructures, corresponding to the formulae R_3Ge_5 and R_4Ge_7, were successfully solved and elucidated for a number of rare earth metals [16 and references herein]. Evidence of an incommensurately modulated superstructure arose from the TEM analysis of a sample of composition La_4Ge_7 [16], but the authors state that this result should be corroborated by further experiments.

Structural data on binary phases stable in the La–Mg–Ge system are summarized in Table 1.

Besides the already cited $La_4Mg_5Ge_6$ and $La_4Mg_7Ge_6$, the existence of the ternary compound La_2MgGe_2 was reported by Kraft et al. [17] in the framework of a systematic investigation on the ternary germanides R_2MgGe_2 (R=Y, La–Nd, Sm, Gd, Tb), all crystallizing in the tetragonal Mo_2FeB_2 structure type. The lanthanum compound is highlighted as an exception in this series of germanides, since it shows a homogeneity range inferred by X-ray diffraction analysis and indicated by the authors with the formula $La_{2+x}Mg_{1-x}Ge_2$, where the *x* limits are not specified; lattice parameters for x= 0.23, 0.25 are reported (see Table 2).

2. Experimental section

2.1 Synthesis

More than fifty alloys were synthesized and characterized to establish the La–Mg–Ge phase relations. Polycrystalline samples were prepared from elemental lanthanum, magnesium (supplied by NewMet Koch, Waltham Abbey, England) and germanium (supplied by MaTecK GmbH, Julich, Germany), all with purity > 99.9 mass %. Stoichiometric amounts of the constituent elements with total weight of about 0.8 g were placed in tantalum crucibles, subsequently arc-sealed to avoid Mg evaporation, and induction melted under a stream of pure argon. In order to ensure homogeneity, each sample was melted three times. The alloys enclosed in crucibles were then sealed in quartz vials, annealed at 500 °C for 7 weeks in a resistance furnace and finally quenched in cold water. With the aim to obtain samples suitable for further structural studies, an alternative synthetic route was performed: a tantalum sealed crucible containing the stoichiometric amounts of the starting elements was closed in an evacuated quartz vial and placed in a resistance furnace equipped with a thermal cycle controller and a mechanical stirring system. A continuous rotation, at a speed of 100 rpm, was applied to the phial during the following thermal cycle: heating from room temperature to a final temperature (T_{max}) depending on the sample composition with a rate of 10 °C/min followed by a slow cooling (0.5 °C/min) to 350 °C. The furnace was then switched off and the alloys were left to cool till room temperature. For comparison some as-cast samples were also analyzed.

2.2 Microstructure and phase analysis

Samples were embedded in a phenolic hot mounting resin with carbon filler, ground by SiC abrasive papers and polished in steps by using diamond pastes with particle size decreasing from 6 to 1 μm, in order to obtain smooth surfaces. Petroleum ether was used as lubricant during polishing and ultrasonic cleaning; alcohol containing lubricants were avoided since many of the examined alloys have proved to be air and moisture sensitive, especially for overall compositions near the La-Ge binary boundary system.

Microstructure examination as well as qualitative and quantitative analyses were performed by a scanning electron microscope (SEM) Zeiss Evo 40 equipped with a Pentafet Link Energy Dispersive X-ray Spectroscopy (EDXS) system managed by the INCA Energy software (Oxford Instruments, Analytical Ltd., Bucks, U.K.).

The EDXS quantitative analyses on La–Mg–Ge alloys are affected by a systematic error due to the energy resolution limit of the spectrometer, which leads to a severe peak overlap between the Mg K/Ge L lines. As a consequence, the magnesium/germanium concentration ratio is overestimated; moreover

the magnitude of the error depends on the composition itself without a regular trend. From our observations the Mg concentration provided by the software is about 3 to 7 at. % higher than the real value when measuring inside the grains of single phases, even higher when measuring the overall alloy compositions. The La content is generally reliable. No significant improvements were obtained by adopting the procedures suggested by the INCA Energy Operator Manual for similar cases, including accurate quant optimization, different quant configurations and profile optimization. Taking into account the previous considerations, the EDXS data recorded on all samples were simply used as guidelines to identify phases, whose exact composition was normally derived from the crystal structure (already known or solved during this work) and in some cases confirmed by Wavelength Dispersive X-ray Spectroscopy (WDXS). The better WDXS spectral resolution generally allowed an improved determination of chemical composition. These analyses were performed on selected alloys using two different instruments: 1) a JEOL 8200 Super Probe Scanning Electron Microscope equipped with five WDXS analyzing spectrometers (standards used for quantitative analysis: phosphate for lanthanum, olivine for magnesium and pure Ge for germanium); 2) a Cameca SX100 electron microprobe system (standard used for quantitative analysis: $LaNi_5$, Ba_6Ge_{25} and Mg_2Si).

2.3 X-ray diffraction analysis

X-ray diffraction on powder samples was performed by means of a diffractometer Philips *X'Pert* MPD (Cu Kα radiation, step mode of scanning) in order to identify phases and to ensure crystal structures of the studied compounds. The X-ray diffraction patterns were indexed by PowderCell [18]; lattice parameters were obtained by a least-squares routine [19].

X-ray diffraction on single crystals was performed on several novel ternary La–Mg–Ge phases. In this work, details of crystal structure solution are presented for the two compounds $La_{11}Mg_2Ge_7$ and $LaMg_{3-x}Ge_2$. Well-shaped single crystals of good quality were extracted from the mechanically fragmented alloys. The crystals were mounted on glass fibers using quick-drying glue. A full-sphere dataset was obtained in routine fashion at ambient conditions on a four-circle Bruker Kappa APEXII CCD area-detector diffractometer equipped by the graphite monochromatized Mo Kα radiation (λ = 0.71073 Å). The instrument was operated in the ω-scan mode. The acquired scans (exposure for 20 s per frame) were integrated using SAINT [20] and the highly redundant final dataset was corrected for Lorentz and polarization effects. Empirical absorption corrections (SADABS) [21] were applied to all data further merged to acceptable R_{sym} values of 0.011 and 0.017 for $La_{11}Mg_2Ge_7$ and $LaMg_{3-x}Ge_2$ respectively. The structures were solved and refined by full-matrix least-squares procedures on $|F^2|$ using SHELX-97 software package [22]. No missed higher crystallographic symmetry in the final models was found by

PLATON [23]. Refined positional parameters have been standardized by STRUCTURE TIDY program [24]. The CIF has also been deposited with Fachinformationszentrum Karlsruhe, 76344 Eggenstein-Leopoldshafen, Germany: depository numbers CSD-426222 and CSD-46223 ($La_{11}Mg_2Ge_7$), CSD-426224 ($LaMg_{3-x}Ge_2$).

4. Results and discussion

Data on ternary phases stable in the La–Mg–Ge system are summarized in Table 2.

4.1 Crystal structure of $La_{11}Mg_2Ge_7$ (τ_1)

Single crystals were extracted from a sample prepared by the alternative synthetic route described in paragraph 2.1 heating up to 950 °C (see microphotograph in fig.S1a).

The systematic absences analysis through the recorded data set was compatible with the only possible centrosymmetric space group $P4_2/ncm$ (№ 138). The major part of starting atomic parameters was deduced from an automatic interpretation of direct methods using SHELX-97 package programs [22]. Taking into account the interatomic distances and isotropic displacement parameters, the preliminary structural model was assumed to contain 3 La, 1 Mg, and 4 Ge fully occupied sites. Nonetheless, four additional prominent peak maxima along the (001) direction at 1/4, 1/4, z with z = 0.06, 0.43, 0.35 0.13 (listed in the intensity decreasing order) were found on the difference Fourier map. A relief mode representation of the latter from $0 \le y \le 0.5$, $0 \le z \le 1$ at $x = 1/4$ is shown in Fig. 1.

The first two peaks were associated to La, and the last two to Mg atoms. The SOFs for all of them were left to vary. As the sum of SOFs for La and Mg species for these sites were close to unity, these conditions were constrained to hold up in further cycles of refinement. A similar disordering phenomenon was observed previously for the related $La_{2-x}Mg_{17+2x}$ binary compound [6]. At the final steps all the atoms (except Mg2-Mg3 couple) were refined anisotropically. The assumed model converged at R1 = 0.036, wR2 = 0.075 and GOF = 1.16 complemented by a flat difference Fourier map. The $La_{11}Mg_2Ge_7$ composition resulting from the obtained model is in very good agreement with the WDXS measured one (see Table 2). Another crystal of the title phase showed the same disordering behaviour. The details of the data collection and refinement for crystal **I** are summarized in Table 3 (analogous details are listed in Table S1 for crystal **II)**. Information on the atomic positions along with isotropic thermal displacement parameters are listed in Table 4. Interatomic distances are listed in Table 5.

The projection of the $La_{11}Mg_2Ge_7$ structure along the c-axis is shown in Fig. 2a: the channels where the above mentioned disordering takes place are highlighted. Searching through Pearson's crystal data

[8] no analogous phases were found, suggesting the title phase being a new structure type. However, numerous R-T-X (R = rare earth metal, *ca*. 60 at.%; T = transition elements; X = Ga, In) tetragonal ternary phases were extracted with the aid of the TOPOS package [25]. The analysis of this subset permitted us to consider all of them as belonging to the Gd_3Ga_2, the Y_3Rh_2 or the $Sm_{26}Co_6Ga_{11}$ parent types. A *Bärnighausen* scheme can help to highlight the structural/compositional relations between phases referring to the same parent type. This approach was applied by Zaremba et al. [26] to the Y_3Rh_2 ternary derivatives. Many of them simply result from the distribution of the three components within the corresponding orbits of the parent type, with T/X statistical mixture in certain sites. For $R_3Rh_{1.3}In_{0.64}$ (R = Gd, Dy) compounds a t2-type symmetry reduction occurs due to an ordered distribution of Rh and In through crystallographic sites. A similar scheme is proposed here (Fig. 3) starting from Gd_3Ga_2. The phase $Ce_{12}Pt_7In$ is a simple ordered substitutional ternary derivative. A $La_{11}Mg_2Ge_7$ hypothetical ordered model is derived through a second order *klassengleiche* symmetry reduction, leading to a primitive tetragonal lattice. This transformation implies the splitting of the 8*g* site into two 4*e* sites, separately occupied by La and Mg. The last row of the scheme represents the real refined structural model of $La_{11}Mg_2Ge_7$. With respect to the calculated one, two more (partially occupied) crystallographic sites are needed to correctly account for the electron density distribution along the *c*-axis. Except for the four 4*e* sites, the positions of remaining atoms are very little shifted with respect to the body-centered lattice of $Ce_{12}Pt_7In$, reflecting the role of the disordering phenomenon on the symmetry breaking. It is interesting to note that magnesium behaves analogously to indium and germanium to platinum, occupying the corresponding sites.

The mentioned subset of compounds can be also conveniently described as belonging to the same homologous series, based on linear alternation of $Ti_3Co_5B_2$ and W_5Si_3-type slabs: this is shown in Fig. 2b for the $La_{11}Mg_2Ge_7$ calculated model, where the ratio of the two fragments is 2:2 (normalized per unit cell). In the same figure the prismatic coordination of Mg atoms by La ($MgLa_8$) in the $Ti_3Co_5B_2$-type slab and the [$GeLa_8$] antiprisms in the W_5Si_3-type slab are also highlighted.

4.2 Crystal structure of $LaMg_{3-x}Ge_2$ (τ_5) as $\sqrt{3}a\times\sqrt{3}a\times 2c$ superstructure

The crystal structure model for this compound was preliminary deduced from powder X-ray diffraction data. The powder patterns taken into considerations for the indexing were of multiphase samples. In any case, the secondary phases of significant contribution show quite simple diffraction patterns, avoiding any overlap with reflections of the compound under study. The powder diffraction analysis permitted to discriminate a set of distinct peaks suitable for further indexing performed with the DICVOL06 program [27]. The indexing was straightforward and the best figure of merit (FOM) was

obtained for a rather small trigonal/hexagonal symmetry unit cell (0.129 nm^3) with a = 0.4528 nm, c = 0.7263 nm. Taking into account the constituents' dimensions, totally 6 atoms may populate the cell. Through the ICSD database [28] 32 structural types were found to be of *hP*6/*hR*6 classes. Constraining the *c/a* ratio to range between 1.4÷1.8 this list of structures was reduced to only 7 candidates. Among these, the most probable parent types were $CaIn_2$ ($P6_3/mmc$-*fb*) and $LaLi_3Sb_2$ (P-3*m*1-d^2ba). Based on our knowledge and previous investigations on R–Mg–Ge compounds [1-4] it is known that neither Mg/Ge nor R/Ge show a tendency to give statistical mixtures. That is why the $LaLi_3Sb_2$-model containing 4 Wyckoff sites was chosen as possible structural model. The formula of the prototype, which is in fair agreement with the electron microprobe analysis results, gave rise to the "$LaMg_3Ge_2$" structural model, which matched pretty well with the observed powder diffraction (see the supplementary data section, Figure S2).

In the meantime, single crystals of the same phase were obtained from a sample subjected to a DTA cycle (heating/cooling rate: 5 °C/min). A temperature of formation of *ca*. 1000 °C was measured. A microphotograph of this sample is shown in figure S1b. The indexation of the collected single-crystal dataset was unambiguous, giving a unit cell six times bigger with respect to the "$LaMg_3Ge_2$" (a = 0.7841, c = 1.4526 nm, V = 0.773 nm^3). Systematic absences analysis indicated only two possible space groups: $P\bar{3}1c$ (No. 163) or $P31c$ (No. 159). A reasonable structural model was easily deduced from an automatic interpretation of direct methods with the SHELX-97 package programs in the centrosymmetric $P\bar{3}1c$ space group, containing 2 La, 1 Ge and 3 Mg sites. This structural model showed good residuals and normal difference Fourier map. The only unusual parameters within this model were the anisotropic displacement parameters for Mg in 2*a* site being two times bigger than the corresponding values for other Mg-sites. In the next cycles of refinement, the occupancy parameter was left to vary for this site, giving a SOF of ~0.8 (the sum formula of this model is $LaMg_{2.6}Ge_2$, Z=3). The final structure model converged at R1 = 0.016, wR2 = 0.038 and GOF = 1.04 with a flat difference Fourier map (for details see Table 3). The atomic positions of the final model are listed in Table 4.

The simple relation between the unit cell dimensions of "$LaMg_3Ge_2$" deduced from powder data and those for $LaMg_{2.6}Ge_2$ (referred further as $LaMg_{3-x}Ge_2$) from X-ray single crystal data aimed us to check the latter to be a $\sqrt{3}a\times\sqrt{3}a\times 2c$ superstructure with regard to the $LaLi_3Sb_2$-type. A useful group-subgroup relationship [29, 30] between the structural models under consideration was established (see Fig. 4). The $LaMg_{3-x}Ge_2$ could be viewed as a result of two subsequent symmetry reduction steps of *klassengleiche* type. The first one (k2) results in a hypothetical structure ($P\bar{3}c1$ space group, has no real representatives) with doubled c parameter. In the following, a (k3) reduction takes place leading to the

$LaMg_{3-x}Ge_2$ superstructure. The number of lost symmetry elements along this relation is well seen from the sketch in Fig. 4 (bottom).

As a consequence, in the superstructure model two general positions (12*i*, occupied by Ge and Mg1) undergo the largest atom shifts; Mg atoms occupying sites derived from the original 1*b* position are located no longer on inversion centers, moreover the 2*d* site is vacant, another 2*a* position is only partially filled; only 1/3 of La atoms maintain inversion centers, but the absolute shift of the heaviest La atoms with the subcell positions is negligible. At this point it became clear that super-reflections are hardly distinguishable from the noise on the registered powder data being of small/zero intensity and single crystal data were of primary importance for the determination of the correct structural model.

To definitely confirm the superstructure, its traces should be found in the diffraction pattern. With the purpose to describe the relationship between supercell-subcell reflections in matrix form it is enough to find an inverse of the group-subgroup transformation shown in Fig. 4 (*i.e.*, the **a**, **b**, **2c** and further **a-b**, **a+2b**, **c** transformations are expressed as $A = \begin{pmatrix} 1 & -1 & 0 \\ 1 & 2 & 0 \\ 0 & 0 & 2 \end{pmatrix}$, so the $A^{-1} = \begin{pmatrix} 2/3 & 1/3 & 0 \\ -1/3 & 1/3 & 0 \\ 0 & 0 & 1/2 \end{pmatrix}$).

From the inverse matrix it follows, that reflections satisfying simultaneously three conditions: $2h+k = 3n$, $-h+k = 3n$, and $l = 2n$ would correspond to those of the subcell. Thus, all remaining spots are super-reflections. In fact, three conditions could be reduced to two independent ones: $2h+k = 3n$ could be viewed as $3h+(-h+k) = 3n$. If $-h+k = 3n$ holds true (second condition), $3h = 3n$ for any h. The relation between subcell and supercell grids in the reciprocal space is well seen along their common ***c**** direction. In Fig. 5a the simulated intensity profiles for the *hk0* zone of the subcell is projected onto the *hk0* zone of the supercell. Instead, along the ***b**** direction there are well distinguished series of two extra lines dividing the space between those of the subcell in three equal parts (Fig. 5b). The precession photos of *hk0* and *h0l* zones, reconstructed from experimental data, are shown in Fig. 6.

Usually, super-reflections are characterized by weak intensity [30]. To evaluate the ratio between mean intensity values for sub/supercell reflections, the list of unique reflections (peaks with $I > 2\sigma(I)$ were considered) was divided into two subsets considering the aforementioned conditions (Table S2, Supplementary data). According to this, the mean intensity of supercell reflections for $LaMg_{3-x}Ge_2$ is about 2% of the corresponding value for subcell. Although being of small intensities, the total number of registered super-reflections is two times bigger than those associated with subcell. Such a strongly different intensity distribution taking place through the collected dataset was also reflected by the uncommon value (1.4) of statistical distribution of normalized *F*-values ($|E^2-1|$).

4.3 Isothermal section at 500 °C

The isothermal section of the La–Mg–Ge phase diagram at 500 °C was determined on the basis of the XRD/SEM/EDXS/WDXS characterization of about 50 samples (Fig. 7a, 7b). A selection of SEM microphotographs of annealed samples is shown in Fig. 8. More details on the synthesized samples and the results of their characterization can be found in the supplementary data (Table S3).

All the binary phases of the boundary systems were confirmed in ternary alloys. The $LaMg_2$ Laves phase, stable in the 775-725 °C temperature range [9], was found to exist in La–Mg–Ge samples annealed at 500 °C; this compound has been reported to be easily stabilized at T<725 °C by a small amount of a third element, such as Si [32]; an analogous effect is known also for $CeMg_2$ [33]. For the binary compounds La_3Ge and LaGe the structural modifications *tP*32–Ti_3P and *oP*8–FeB, respectively, were detected in all the annealed ternary alloys.

As it was outlined in the introduction, in the 60-65 at.% Ge range of the La–Ge system the Ge vacancies ordering phenomenon leads to many related structures difficult to discern. This is the reason why only the defect versions of the α-$ThSi_2$ and the α-$GdSi_2$-type structures were used as structural models for phase relations studies. Based on EDXS analyses, a phase of formula $LaGe_{2-x}$ was indicated, extending from about 62 to 64 at. % Ge at 500 °C. Powder diffraction patterns containing the Ge-rich $LaGe_{2-x}$ were successfully indexed with the orthorhombic prototype, showing well resolved pairs of reflections (for example the 0 1 5/1 0 5 and 0 2 0/2 0 0); on the other hand for the Ge-poor $LaGe_{2-x}$ it was not possible to distinguish between the tetragonal structure and the orthorhombic one with $a \approx b$ (pseudo-tetragonal), so that the tetragonal model was accepted. Considering that the temperature of the $LaGe_{2-x}$ orthorhombic → tetragonal transition increases from 425 to 635 °C when increasing the Ge content [14], it is nevertheless possible that at 500 °C both structures are stable.

No ternary solid solutions were indicated in Fig. 7b. The EDXS analyses on the binary La–Ge phases usually showed the presence of an amount of Mg oscillating from about 3 to 7 at.%, altering their correct stoichiometry. The presence of Mg was ascribed to the quantitative measurement error discussed in the experimental section, taking into account that a) omitting magnesium the composition fits the correct stoichiometry, b) the lattice parameters are in good agreement with those reported for binaries. Anyway a little solubility of Mg in these phases cannot be excluded.

The La–Mg–Ge system is rich in stoichiometric ternary phases, whose crystal structures and measured compositions are listed in Table 2. Except for $La_6Mg_{23}Ge$ (τ_6), the other compounds are located around the 35 at.% or 66 at.% Ge isoconcentration lines.

The La-richest ternary compound is τ_1-$La_{11}Mg_2Ge_7$, crystallizing in its own structure type (see paragraph 4.1). Microscopic observations indicate that τ_1 forms uncongruently in a reaction involving the La_5Ge_3 binary phase (of congruent formation at 1475 °C).

The $0 \le x \le 0.25$ homogeneity range is proposed for the phase τ_2-$La_{2+x}Mg_{1-x}Ge_2$ (*tP*10-Mo_2FeB_2), based both on our and literature data. In agreement with [17], the *a* parameter was found to decrease on increasing the Mg/La ratio, whereas the *c* parameter does not change noticeably (Table 2). The stability of τ_2 is reflected in the high number of tie-lines converging on it.

Crystal and electronic structure properties of the ternary compounds τ_3-$La_4Mg_5Ge_6$ and τ_4-$La_4Mg_7Ge_6$ were discussed in [4]. These phases are involved in two three-phase fields ($\tau_2 + \tau_3 + \tau_4$ and $\tau_3 + \tau_4 + \tau_5$) whose vertices are ternary compounds compositionally quite close. At earlier stages of current research, these features made it difficult to obtain samples in equilibrium, to distinguish between the novel ternary compounds and to get specimens suitable for structural studies. In particular, the τ_5-$LaMg_{3-x}Ge_2$ compound was always present in a small amount in 500 °C annealed samples, and only after a controlled thermal cycle in DTA up to the temperature of about 1300 °C a higher yield of it was obtained. The off-stoichiometry of τ_5 is definitely determined by the X-ray characterization, even if the EDXS and WDXS results do not adequately account for it; the full characterization of the analogous non-stoichiometric phase $LaMg_{3-x}Sn_2$ (EDXS analysis: $La_{18.6}Mg_{45.2}Sn_{36.2}$), which is currently under study in our laboratory, strengthens this conclusion.

Electron structure calculations for $LaMg_{3-x}Ge_2$ are in progress, also aimed to compare results with the DOS and COHP curves obtained by Suen et al. [1] for the hypothetical compound "$La_5Mg_8Ge_8$" (close in composition to τ_3, τ_4 and τ_5), whose existence was excluded under the conditions considered in this work.

A small amount of Ge stabilizes the ternary phase τ_6-$La_6Mg_{23}Ge$, which is in equilibrium with the close $LaMg_3$ binary phase. The X-ray diffraction pattern of an annealed polycrystalline sample, containing an elevated fraction of this phase, was successfully indexed on the basis of a structural model obtained by substituting Si for Ge in the structure of the $La_6Mg_{23}Si$ compound (space group: $Fm\bar{3}m$, *cF*120- Zr_6SiZn_{23}, f^2edba, Z=4) [33]. This model was chosen based on the EDXS measured composition of τ_6 and the chemical similarity of the component metals. A Rietveld refinement was performed using the FULLPROF [34] program; least-squares refinement cycles converged to $R_F = 0.05$ and $R_B = 0.07$ for the title phase. The observed, calculated and differential X–ray powder diffraction patterns of this sample are plotted in Fig. S3. The refined lattice parameter is a = 1.46694(6) nm; fractional atomic positions for all atoms are: La – 24*e* (x, 0, 0), x=0.2914(5); Mg1 – 24*d* (0, 1/4, 1/4); Mg2 – 32*f* (x, x, x), x = 0.329(1); Mg3 – 32*f* (x, x, x), x = 0.117(1); Mg4 – 4*b* (1/2, 1/2, 1/2); Ge – 4*a* (0, 0, 0).

The Zr_6SiZn_{23} structure type is an interstitial variant of the Th_6Mg_{23} cubic structure; new representatives of it, belonging to the $Ce_6Mg_{23}X$ series (where X=elements of IV and V-th groups), were recently studied and the structural relationships between $LaMg_3$ and $R_6Mg_{23}X$ compounds were discussed [35]. One of the distinctive peculiarities of the τ_6 structure is the presence of $GeLa_6$ regular octahedra, which are quite uncommon for intermetallics.

In the Ge-rich corner two novel ternary compounds were detected: τ_7-La_4MgGe_{10-x} (x=0.37) and τ_8-La_2MgGe_6. The microstructure appearance of samples in this region indicates that both ternary phases form incongruently: in fact τ_7 is often visible as a slightly darker border around $LaGe_{2-x}$ (congruent formation at 1500 °C) and τ_8 in turn as a darker border around τ_7. For this reason it is not trivial to obtain τ_7 or τ_8 single phase alloys, and their crystal structures were solved by X-ray diffraction analysis of single crystals selected from multi-phase samples where they were not present together. The τ_7-La_4MgGe_{10-x} (x=0.37) crystallizes in its own structure type and is characterized by a Ge-deficiency; τ_8-La_2MgGe_6 belongs to the numerous family of the $Ce_2(Ga_{0.1}Ge_{0.9})_7$-type compounds [36]. The compositions resulting from the structure models are in good agreement with the WDXS measurements, whereas EDXS show a significant Mg overestimation. Details of crystal structure solution, crystal structure analysis and electronic structure calculations on these Ge-rich compounds became the object of a forthcoming manuscript.

5. Conclusions

The La–Mg–Ge phase relations were studied ~~in the whole composition range~~ and the whole isothermal section at 500 °C was constructed. The interaction of components in this ternary system leads to the formation of eight ternary compounds, most of which were found and structurally characterized during this work. All compounds but $La_6Mg_{23}Ge$ (τ_6) contain more than 30 at. % Ge, and are distributed along the 35 at.% ($La_{11}Mg_2Ge_7$ (τ_1), $La_{2+x}Mg_{1-x}Ge_2$ (τ_2), $La_4Mg_5Ge_6$ (τ_3), $La_4Mg_7Ge_6$ (τ_4), $LaMg_{3-x}Ge_2$ (τ_5)) or 66 at.% Ge (La_4MgGe_{10-x} (τ_7), La_2MgGe_6 (τ_8)) isoconcentration lines. Except for $La_{2+x}Mg_{1-x}Ge_2$ (τ_2), the other phases are point compounds; analogously, the binary compounds do not show a remarkable tendency to dissolve the third element. A half of ternaries crystallize in their own structure type, enriching the crystallochemistry of germanides. Disordering phenomena were observed for a number of La–Mg–Ge phases:

- $La_{11}Ge_7Mg_2$ is characterized by the presence of “channels” along the (001) direction filled by La/Mg in partially occupied crystallographic sites.
- $LaMg_{3-x}Ge_2$ is a $\sqrt{3}a\times\sqrt{3}a\times 2c$ superstructure of the $LaLi_3Sb_2$ structure type, where the 2*d* and 2*a* Mg sites (arising from the split original 1*b* site) are empty and partially occupied, respectively.

- La_4MgGe_{10-x} (whose crystal structure will be shown and discussed in our next work) could be viewed as a ternary example of the vacancy ordering phenomenon common for binary R-Ge compounds in the 60-66.7 at.% Ge compositional range.

The previously obtained results on the crystal structure and chemical bonding of $La_4Mg_5Ge_6$ and $La_4Mg_7Ge_6$ complemented with these new data provides a good basis to study the interplay between composition, crystal structure and chemical bonding peculiarities for La–Mg–Ge ternary compounds and become the scope of a forthcoming paper.

APPENDIX A. SUPPLEMENTARY DATA

Supplementary data associated with this article can be found in the online version at ...

ACKNOWLEDGMENTS

The authors thank Dr. Ulrich Burkhardt, (*MPI-CPfS, Dresden, Germany*) for providing access to WDXS equipment.

References

[1] Suen, N.-T.; Bobev, S. *Eur. J. Inorg. Chem.* **2012**, 4141-4148.

[2] Guo, S.-P.; You, T.-S.; Jung, Y-H.; Bobev, S. *Inorg. Chem.* **2012**, *51*, 6821−6829.

[3] Suen, N.-T.; Bobev, S. *Inorg. Chem.* **2013**, *52*, 12731−12740.

[4] Solokha, P.; De Negri, S.; Skrobanska, M.; Saccone, A.; Pavlyuk, V.; Proserpio, D.M. *Inorg. Chem.* **2012**, *51*, 207−214.

[5] Berche, A.; Benigni, P.; Rogez, J.; Record, M.C. *J. Therm. Anal. Calorim.* **2012**, *107*, 797-807.

[6] De Negri, S.; Solokha, P.; Pavlyuk, V.; Saccone, A. *Intermetallics* **2011**, *19*, 671-680.

[7] Denys, R.V.; Poletaev, A.A.; Solberg, J.K.; Tarasov, B.P.; Yartys, V.A., *Acta Materialia* **2010**, *58*, 2510–2519.

[8] Villars, P.; Cenzual, K. Pearson's Crystal Data, Release 2013/14, ASM International, Ohio, USA**.**

[9] Massalski, T.B. Binary Alloy Phase Diagrams, Vol. 1-3. American Society for Metals. Metals Park, Oh 44073, USA, 1990;

[10] Garde, C.S.; Ray, J.; Chandra, G. *J. Alloys Compd*. **1993**, *198*, 165-172.

[11] Gryniv, J.A.; Pecharskii, V.K.; Yarmdyuk, Y.P.; Bodak, O.J.; Bruskov, V.A. *Sov. Phys. Crystallogr.* **1987**, *32*, 460-461.

[12] Guloy, A.M.; Corbett, J.D. *Inorg. Chem.* **1993**, *32*, 3532-3540.

[13] Mattausch, H.; Simon, A. *Z. Naturforsch. B* **2004**, *59*, 559-561.

[14] Guloy, A.M.; Corbett, J.D. *Inorg. Chem.* **1991**, *30*, 4789-4794;

[15] Venturini, G.; Ijjaali, I.; Malaman, B. *J.Alloys Compd.* **1999**, *289*, 168-177.

[16] Zhang, J.; Tobash, P.H.; Pryz, W.D.; Buttey, D.J.; Hur, N.; Thompson, J.D.; Sarrao, J.L.; Bobev S. *Inorg. Chem.* **2013**, *52*, 953−964.

[17] Kraft, R.; Pöttgen, R. *Monatshefte für Chemie* **2004**, *135*, 1327-1334;

[18] Kraus, W.; Nolze, G. *J. Appl. Cryst.* **1996**, *29*, 301-303.

[19] Schwarzenbach, D. LATCON: Refine Lattice Parameters, University of Lausanne, Lausanne, Switzerland 1966.

[20] Bruker. AXS Inc. (**2011**). SAINT. Bruker. AXS Inc., Madison, WI, USA.

[21] Bruker. AXS Inc. (**2011**). SADABS. Bruker. AXS Inc., Madison, WI, USA.

[22] (a) Sheldrick G. M. *SHELXS–97: Program for the Solution of Crystal Structures*; University of Göttingen: Germany, 1997. (b) Sheldrick G. M. *SHELXL–97: Program for Crystal Structure Refinement*; University of Göttingen: Germany, **1997**.

[23] Spek A. L. PLATON, a multipurpose crystallographic tool. Utrecht University, The Netherlands, 2002

[24] Gelato, L.; Parthé, E. *J. Appl. Crystallogr.* **1987**, *20*, 139-143.

[25] Blatov, V.A. Shevchenko, A. P. Serezhkin, V.N. *J. Appl. Cryst.* **2000**, *33 (4)*, 1193.

[26] Zaremba, R.; Rodewald, U. Ch.; Zaremba, V.I.; Pöttgen, R. *Z. Naturforsch. B.* **2007**, *62*, 1397-1406.

[27] Boultif, A.; Louër, D. *J. Appl. Crystallogr.* **1991**, *24*, 987-993.

[28] Belsky A.; Hellenbrandt M.; Karen V.L.; Luksch P. *Acta Cryst. B* **2002**, *58*, 364–369.

[29] Wondratshek H.; Müller U. (Ed.). International *Tables for Crystallography, Vol. A1: Symmetry relations between space groups*, Kluwer Academic Publishers, Dordrecht, **2004**.

[30] Müller U. *Symmetry Relationships between Crystal Structures. Applications of Crystallographic Group Theory in Crystal Chemistry*, Oxford University Press, 2013.

[31] Sheldrick G.M. XPREP 6.12, SHELXTL, Bruker-AXS.

[32] De Negri, S.; Saccone, A.; Delfino, S. *Calphad* **2009**, *33*, 44-49.

[33] Zmii, F.; Gladyshevskiy, E.I. *Visn. L'viv Univ., Ser. Khim.* **1974**, *15*, 24-26 (in ukrainian).

[34] Rodriguez-Cavajal, J. "Recent developments in the program FullProf", Newsletter **2001**, *26*, 12-19.

[35] F. Wrubl et al., unpublished results.

[36] A. Saccone, P. Solokha, S. De Negri, M. Skrobanska, D. M. Proserpio, Book of Abstracts of 18th International Conference on Solid Compounds of Transition Elements, Lisbon, (Portugal), 31 march-5 april 2012, p. 120.

Figure Captions

Figure 1. Difference Fourier map of the preliminary model of $La_{11}Mg_2Ge_7$ in the region $0 \le y \le 0.5$, $0 \le z \le 1$ at $x = 1/4$.

Figure 2. a) Projection of the $La_{11}Mg_2Ge_7$ structure along the *c*-axis; the channels hosting the disordered positions are highlighted. b) $Ti_3Co_5B_2$ and W_5Si_3-type slabs and their linear intergrowth in the crystal space of the $La_{11}Mg_2Ge_7$ calculated model.

Figure 3. Group-subgroup relation in the *Bärnighausen* formalism for the $Gd_3Ga_2 \rightarrow La_{11}Mg_2Ge_7$ structural models. The type and order of the symmetry reduction and the evolution of the atomic parameters are shown.

Figure 4. Group-subgroup relation in the *Bärnighausen* formalism for the $LaLi_3Sb_2$ and $LaMg_{3-x}Ge_2$ structures. The indexes of the symmetry reductions and the evolution of the atomic parameters are given. In the bottom the relation between unit cells metrics for structures under discussion together with the number/type of symmetry elements for respective space groups are shown.

Figure 5. Simulated by XPREP [31] intensity profiles for *hk0* and *h0l* zones of $LaMg_{3-x}Ge_2$ compound (red color grid). *a) hk0* zone of subcell (green color grid) projected onto the supercell one. *b)* the weak supercell extra lines reflections are indicated by green arrows within the *h0l* zone.

Figure 6. Observed and simulated intensity profiles for *hk0* and *h0l* zones demonstrate the presence of weak super-reflections. To the right are shown the 3D images of respective blue area highlighting the difference of peaks intensities.

Figure 7. a) Nominal compositions of the La–Mg–Ge alloys (▲: three-phase samples, □: two-phase samples, ◇: more than three phases samples). Red frames distinguish samples prepared by slow cooling method. Numbers correspond to samples listed in the supplementary data (Table S3). b) Isothermal section of the La–Mg–Ge system at 500 °C.

Figure 8. Micrographs (SEM-BSE mode) of selected La-Mg-Ge samples annealed at 500 °C: (a) $La_{66}Mg_{11}Ge_{23}$ alloy (bright phase: La_3Ge, grey phase: La_5Ge_3, dark phase: LaMg); (b) $La_{42}Mg_7Ge_{51}$ alloy (bright phase: LaGe, grey phase: $LaGe_{2-x}$, dark phase: τ_2-$La_{2+x}Mg_{1-x}Ge_2$); (c) $La_{33}Mg_{24}Ge_{43}$ alloy (bright phase: $LaGe_{2-x}$, grey phase: τ_2-$La_{2+x}Mg_{1-x}Ge_2$, dark phase: τ_3-$La_4Mg_5Ge_6$); (d) $La_{28}Mg_{52}Ge_{20}$ alloy (bright phase: τ_2-$La_{2+x}Mg_{1-x}Ge_2$, grey phase: τ_6-$La_6Mg_{23}Ge$, dark phase: La_2Mg_{17}); (e) $La_5Mg_{80}Ge_{15}$ alloy (bright phase: τ_4-$La_4Mg_7Ge_6$, grey phase: Mg_2Ge, dark phase: Mg); (f) $La_5Mg_{80}Ge_{15}$ alloy (bright phase: τ_7-La_4MgGe_{10-x}, grey phase: τ_8-La_2MgGe_6, dark phase: Ge, white particles of oxide).

Table 1. Crystallographic data on binary phases stable in the La–Mg–Ge system

Phase	Pearson symbol–Prototype	Lattice parameters (nm)			Comments
		a	b	c	
LaMg	*cP*2–CsCl	0.3970(3)			[8]
		0.3965(1)			this work
$LaMg_2$	*cF*24-$MgCu_2$	0.8810(2)			[8]
		0.87988(8)			this work
$LaMg_3$	*cF*16–BiF_3	0.7494(2)			[8]
		0.7517(1)			this work
La_5Mg_{41}	*tI*92-Ce_5Mg_{41}	1.4822		1.0468	[8]
La_2Mg_{17}	*hP*42-3.64–$CeMg_{10.3}$	1.0388(2)		1.0263(2)	[6]
		1.033(1)		1.024(1)	this work
$LaMg_{\sim 11}(LaMg_{12})$	*oI*346-10.32–$LaMg_{\sim 11}$	1.03391(5)	1.03554(5)	7.7484(4)	[8]
Mg_2Ge	*cF*12–CaF_2	0.63849(4)			[8]
		0.63915(8)			this work
La_3Ge (α)	*oP*16–Fe_3C	0.7416(20)	0.9954(25)	0.6497(31)	[8]
La_3Ge (β)	*tP*32–Ti_3P	1.2741(2)		0.6298(1)	[8]
		1.273(1)		0.628(1)	this work
La_5Ge_3	*hP*16–Mn_5Si_3	0.89409(5)		0.68784(6)	[8]
		0.8946(3)		0.6893(3)	this work
La_4Ge_3	*cI*28–Th_3P_4	0.93563(4)			[8]
		0.9354(1)			this work
La_5Ge_4	*oP*36–Sm_5Ge_4	0.8065(1)	1.5474(2)	0.8172(2)	[8]
		0.805(2)	1.550(2)	0.8170(9)	this work
LaGe	*oP*8–FeB	0.8488(1)	0.4128(1)	0.6122(1)	[8]
		0.8467(1)	0.41305(8)	0.6110(2)	this work
LaGe	*oS*16-LaSi	0.45590(10)	1.3766(2)	0.6745(2)	[8]
$LaGe_{2-x}$ (α)	*oI*12–α$GdSi_2$	0.4312(1)	0.4408(1)	1.4188(1)	x=0.33
		0.42680(7)	0.42735(6)	1.4404(1)	x=0.40
		0.4325(1)	0.4419(1)	1.4161(6)	x=0.2, this work
$LaGe_{2-x}$ (β)	*tI*12–$ThSi_2$	0.4400(1)		1.4175(2)	x=0.33
		0.4274(1)		1.4389(2)	x=0.40
		0.4274(1)		1.435(1)	x=0.35, this work

Table 2. Ternary phases in the La–Mg–Ge system.

Phase	WDXS composition *EDXS composition*	Space group Pearson symbol–Prototype	Lattice parameters (nm)			Comments
			a	*b*	*c*	
τ_1-$La_{11}Mg_2Ge_7$	$La_{54.8}Mg_{10.0}Ge_{35.1}$ *$La_{53.4}Mg_{13.1}Ge_{33.5}$*	*$P4_2/ncm$* (№ 138) *tP*88-8–$La_{11}Mg_2Ge_7$	1.21338(5)		1.57802(6)	
τ_2-$La_{2+x}Mg_{1-x}Ge_2$ $0 \le x \le 0.25$	$La_{41.0}Mg_{20.7}Ge_{38.3}$* *$La_{39.0}Mg_{22.8}Ge_{38.2}$**	*P4/mbm* (№ 127) *tP*10–Mo_2FeB_2	0.77052(7)[a] 0.75906(6)		0.4474(1)[a] 0.44856(8)	x=0.25 x=0
τ_3-$La_4Mg_5Ge_6$	$La_{28.6}Mg_{32.3}Ge_{39.1}$ *$La_{24.7}Mg_{39.1}Ge_{36.2}$*	*$Cmc2_1$* (№ 36) *oS*60–$Gd_4Zn_5Ge_6$	0.45030(7)[b]	2.0085(3)[b]	1.6207(3)[b]	
τ_4-$La_4Mg_7Ge_6$	$La_{24.1}Mg_{42.4}Ge_{33.5}$ *$La_{22.2}Mg_{44.7}Ge_{33.1}$*	*C12/m1* (№ 12) *mS*34–$La_4Mg_7Ge_6$	1.6878(3)[b]	0.44702(9)[b]	1.2660(3)[b]	β=122.25°(3)[b]
τ_5-$LaMg_{3-x}Ge_2$ x=0.407(5)	$La_{16.3}Mg_{50.0}Ge_{33.7}$ *$La_{16.8}Mg_{49.6}Ge_{33.6}$*	*$P\bar{3}1c$* (№ 163) *hP*34-0.44–$LaMg_{3-x}Ge_2$	0.78408(4)		1.45257(7)	
τ_6-$La_6Mg_{23}Ge$	- *$La_{21.0}Mg_{75.0}Ge_{4.0}$*	*Fm-3m* (№ 225) *cF*120–$Zr_6Zn_{23}Si$	1.46694(6)			
τ_7-La_4MgGe_{10-x} x=0.37(1)	$La_{26.8}Mg_{7.7}Ge_{65.5}$ *$La_{25.3}Mg_{13.3}Ge_{61.5}$*	*C2/m* (№ 12) *mS*60-1.46–La_4MgGe_{10-x}	0.88403(8)	0.86756(8)	1.7709(2)	β=97.16°(1)
τ_8-La_2MgGe_6	$La_{21.8}Mg_{13.0}Ge_{65.2}$ *$La_{20.7}Mg_{17.7}Ge_{61.6}$*	*Cmce* (№ 64) *oS*72–$Ce_2(Ga_{0.1}Ge_{0.9})_7$	0.89889(11)	0.85172(11)	2.1064(3)	

[a] Data taken after [15] [b]Data taken after [2]

*measured compositions for the Mg-rich side of the phase (x=0)

Table 3. Crystallographic data for the $La_{11}Ge_7Mg_2$ (crystal **I**) and $LaMg_{3-x}Ge_2$ (x=0.407(5)) single crystals together with some experimental details of the structure determination.

Empirical formula	$La_{11}Ge_7Mg_2$	$LaMg_{3-x}Ge_2$
Structure type	$La_{11}Ge_7Mg_2$	$LaMg_{3-x}Ge_2$
Crystal system	Tetragonal	Trigonal
Space group	$P4_2/ncm$ (№ 138)	$P\bar{3}1c$ (№ 163)
Pearson symbol, Z	*tP*88-8, 4	*hP*34-0.44, 6
Unit cell dimensions:		
a, nm	1.21338(5)	0.78408(4)
c, nm	1.57802(6)	1.45257(7)
V, nm^3	2.3233(2)	0.77337(7)
Calc. density (D_{calc}, $g \cdot cm^{-3}$)	5.96	3.07
Abs. coefficient (μ, mm^{-1})	28.647	13.269
Total no. reflections	38515	12926
Independent reflections	1271 (R_{int} = 0.0309)	692 (R_{int} = 0.0285)
Reflections with $I > 2\sigma(I)$	1207 (R_{sigma} = 0.0108)	479 (R_{sigma} = 0.0175)
Data/parameters	1271/66	692/30
Goodness-of-fit on F^2	1.25	1.04
Final *R* indices; R_1/wR_2	0.0338/0.0682	0.0164/0.0381
R indices (all data)	0.0354/0.0688	0.0306/0.0420
$\Delta\rho_{fin}$ (max/min), $e \cdot nm^{-3}$ ($\times 10^3$)	2.83/-2.49	0.64/-0.74

Table 4. Atomic coordinates and equivalent isotropic displacement parameters (Å^2) for the $La_{11}Ge_7Mg_2$ (crystal I) and $LaMg_{3-x}Ge_2$, x=0.407(5) single crystals.

Atom	**Wyck. site**	**Site**	***x/a***	***y/b***	***z/c***	**SOF**	**U_{eq}, Å^2**
$La_{11}Mg_2Ge_7$ (origin choice 2)							
La1	16*j*	1	0.17768(5)	0.54609(5)	0.10789(4)		0.0171(2)
La2	16*j*	1	0.18317(5)	0.53685(5)	0.38910(4)		0.0167(2)
La3	8*i*	..*m*	0.08429(6)	0.08429(6)	0.24550(5)		0.0205(2)
Ge1	4*a*	2.22	3/4	1/4	0		0.0157(7)
Ge2	8*i*	..*m*	0.1364(2)	0.1364(2)	0.7417(2)		0.0240(4)
Ge3	8*i*	..*m*	0.0890(2)	0.0890(2)	0.44395(9)		0.0207(4)
Ge4	8*i*	..*m*	0.0705(2)	0.0705(2)	0.05289(1)		0.0224(4)
Mg1	4*b*	-4..	3/4	1/4	3/4		0.0168(1)
La4	4*e*	2.*mm*	1/4	1/4	0.0647(2)	0.765(6)	0.0131(5)
La5	4*e*	2.*mm*	1/4	1/4	0.4270(5)	0.235(6)	0.037(2)
Mg2	4*e*	2.*mm*	1/4	1/4	0.3608(6)	0.69(2)	0.010(3)
Mg3	4*e*	2.*mm*	1/4	1/4	0.112(2)	0.31(2)	0.019(7)
$LaMg_{3-x}Ge_2$ x= 0.407(5)							
La1	2*b*	-3..	0	0	0		0.0076(1)
La2	4*f*	3..	1/3	2/3	0.00323(1)		0.0082(1)
Ge1	12*i*	1	0.01731(4)	0.33630(2)	0.12744(2)		0.0103(1)
Mg1	12*i*	1	0.3591(2)	0.0299(2)	0.32406(7)		0.0170(2)
Mg2	2*c*	3.2	1/3	2/3	1/4		0.0157(4)
Mg3	2*a*	3.2	0	0	1/4	0.779(5)	0.0166(7)

Table 5. Interatomic distances for τ_1-$La_{11}Mg_2Ge_7$ and τ_5-$LaMg_{3-x}Ge_2$ (* refers to the distances between atoms occupying sites with SOF<1)

$La_{11}Mg_2Ge_7$								
Atom 1	Atom 2	Dist. [nm]	Atom 1	Atom 2	Dist. [nm]	Atom 1	Atom 2	Dist. [nm]
La1–	Ge2	0.3100(2)	Ge2–	Mg2	0.2709(7)	Mg1–	4La1	0.3453(1)
	Ge1	0.3129(1)		Mg3	0.2826(23)		4La2	0.3488(1)
	Ge3	0.3246(2)		2La1	0.3100(2)	La4–	Mg3	0.0746(32)*
	Ge3	0.3378(1)		2La2	0.3186(2)		La5	0.2173(8)*
	Mg1	0.3453(1)		La4	0.3406(2)		2Ge4	0.3085(1)
	Ge4	0.3477(1)		2La3	0.3448(2)		Mg2	0.3218(10)*
La2–	Ge2	0.3186(2)	Ge3–	La5	0.2775(2)		2Ge3	0.3356(2)
	Ge4	0.3201(2)		Mg2	0.3058(4)		2Ge2	0.3406(2)
	Ge1	0.3226(1)		La3	0.3133(2)	La5–	Mg2	0.1045(12)*
	Ge4	0.3238(1)		2La1	0.3246(2)		La4	0.2173(8)*
	Ge3	0.3274(1)		2La2	0.3274(1)		2Ge3	0.2775(2)
	Mg1	0.3488(1)		La4	0.3356(2)		Mg3	0.2919(33)*
La3–	Ge4	0.3049(2)		2La1	0.3378(1)	Mg2–	La5	0.1045(12)*
	Ge3	0.3133(2)	Ge4–	Ge4	0.2940(2)		2Ge2	0.2709(7)
	Mg2	0.3376(5)		La3	0.3049(2)		2Ge3	0.3058(4)
	2Ge2	0.3448(2)		La4	0.3085(1)		La4	0.3218(10)*
Ge1–	4La1	0.3129(1)		2La2	0.3201(2)		2La3	0.3376(5)
	4La2	0.3226(1)		Mg3	0.3218(9)	Mg3–	La4	0.0746(32)*
				2La2	0.3238(1)		2Ge2	0.2826(23)
				2La1	0.3477(1)		La5	0.2919(33)*
							2Ge4	0.3218(9)

$LaMg_{3-x}Ge_2$								
Atom 1	Atom 2	Dist. [nm]	Atom 1	Atom 2	Dist. [nm]	Atom 1	Atom 2	Dist. [nm]
La1–	6Ge1	0.3169(1)	Ge1–	Mg1	0.2669(1)	Mg1–	Ge1	0.2669(1)
La2–	2Ge1	0.3112(1)		Mg1	0.2687(1)		Ge1	0.2687(1)
	Ge1	0.3113(1)		Mg1	0.2798(1)		Ge1	0.2798(1)
	Ge1	0.3331(1)		Mg1	0.2877(1)		Ge1	0.2877(1)
	Ge1	0.331(1)		Mg2	0.3098(1)		Mg3	0.2912(1)
	Ge1	0.332(1)		La2	0.3112(1)		Mg2	0.2955(1)
				Mg3	0.3128(1)		Mg1	0.3184(1)
				La1	0.3169(1)		Mg1	0.3256(1)
				La2	0.3331(1)	Mg2–	4Mg1	0.2955(1)
							2Mg1	0.2956(1)
							4Ge1	0.3098(1)
							2Ge1	0.3099(1)
						Mg3–	6Mg1	0.2912(1)
							6Ge1	0.3128(1)

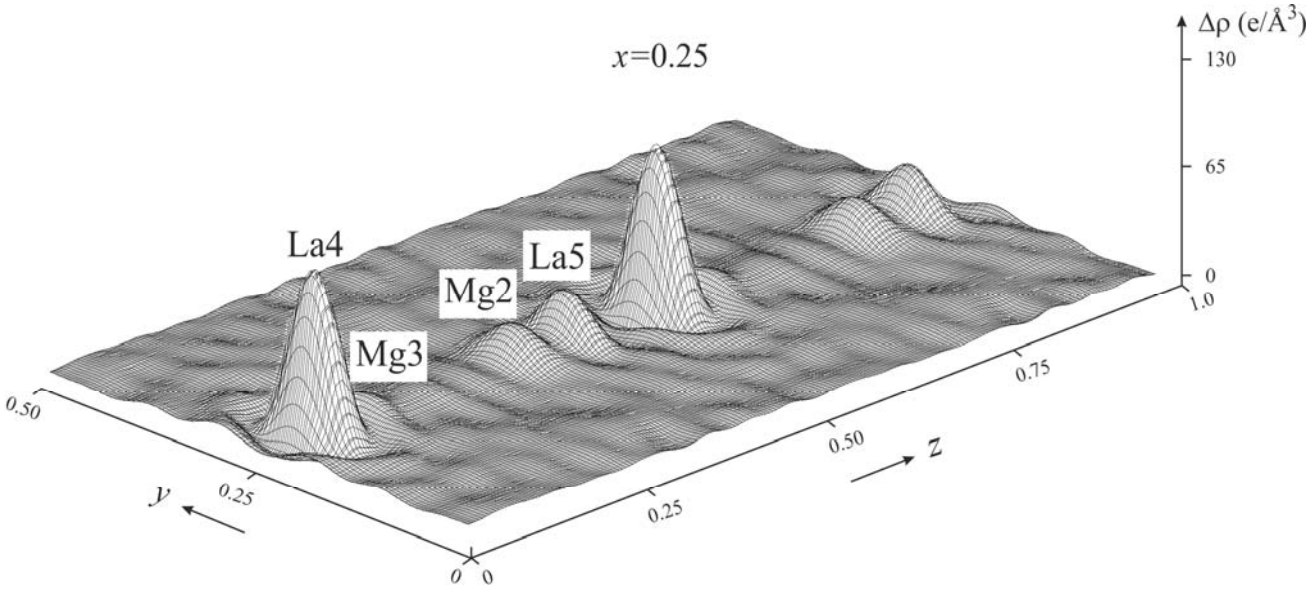

Fig. 1.

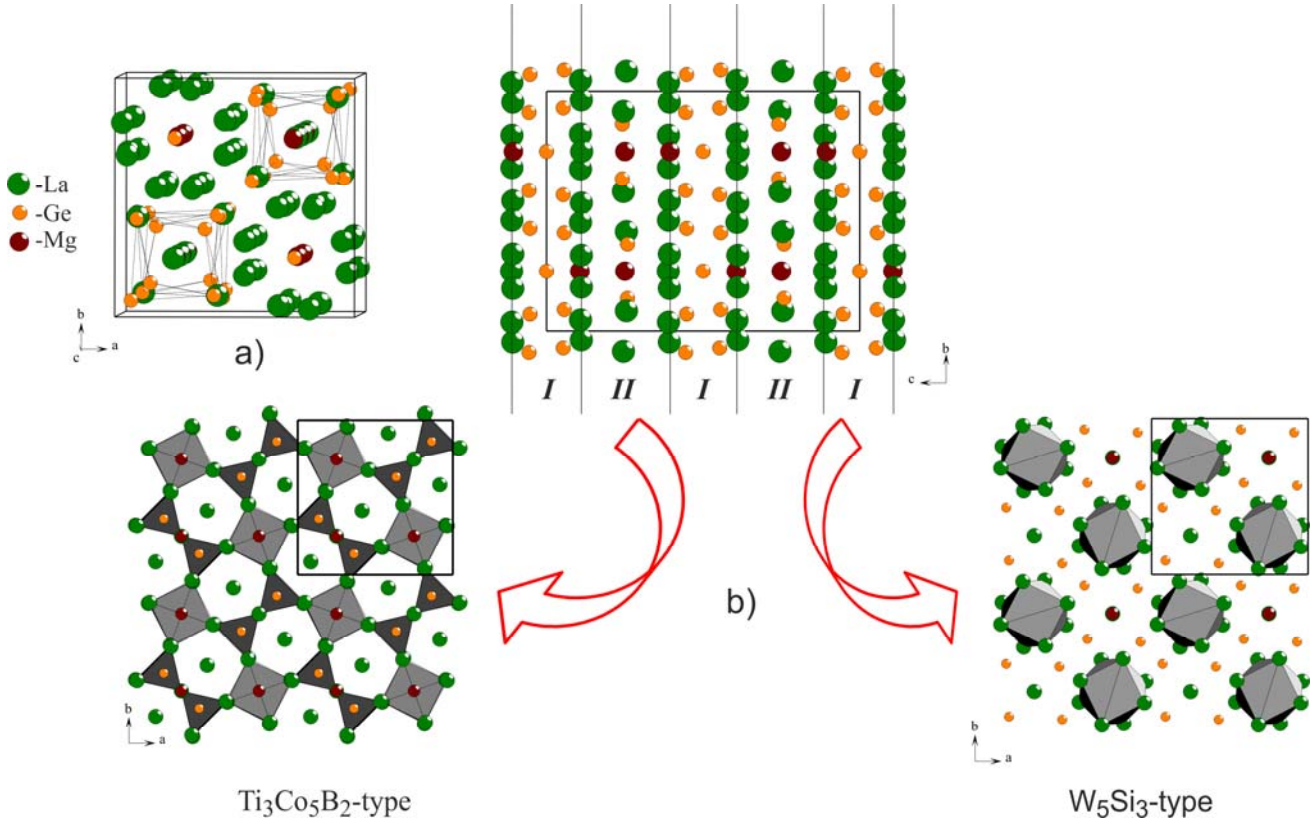

Fig. 2.

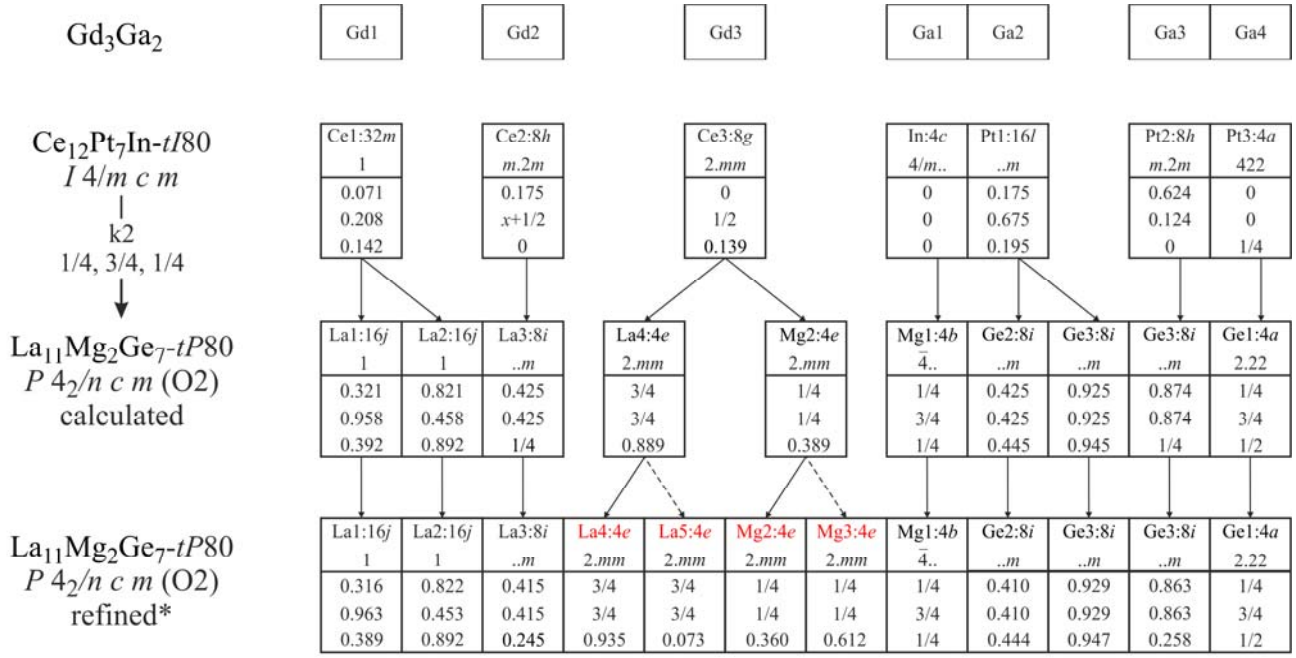

* in the manuscript fractional atomic positions values are standardized by STRUCTURE TIDY; positions partially occupied in the structure are marked in red

Fig. 3.

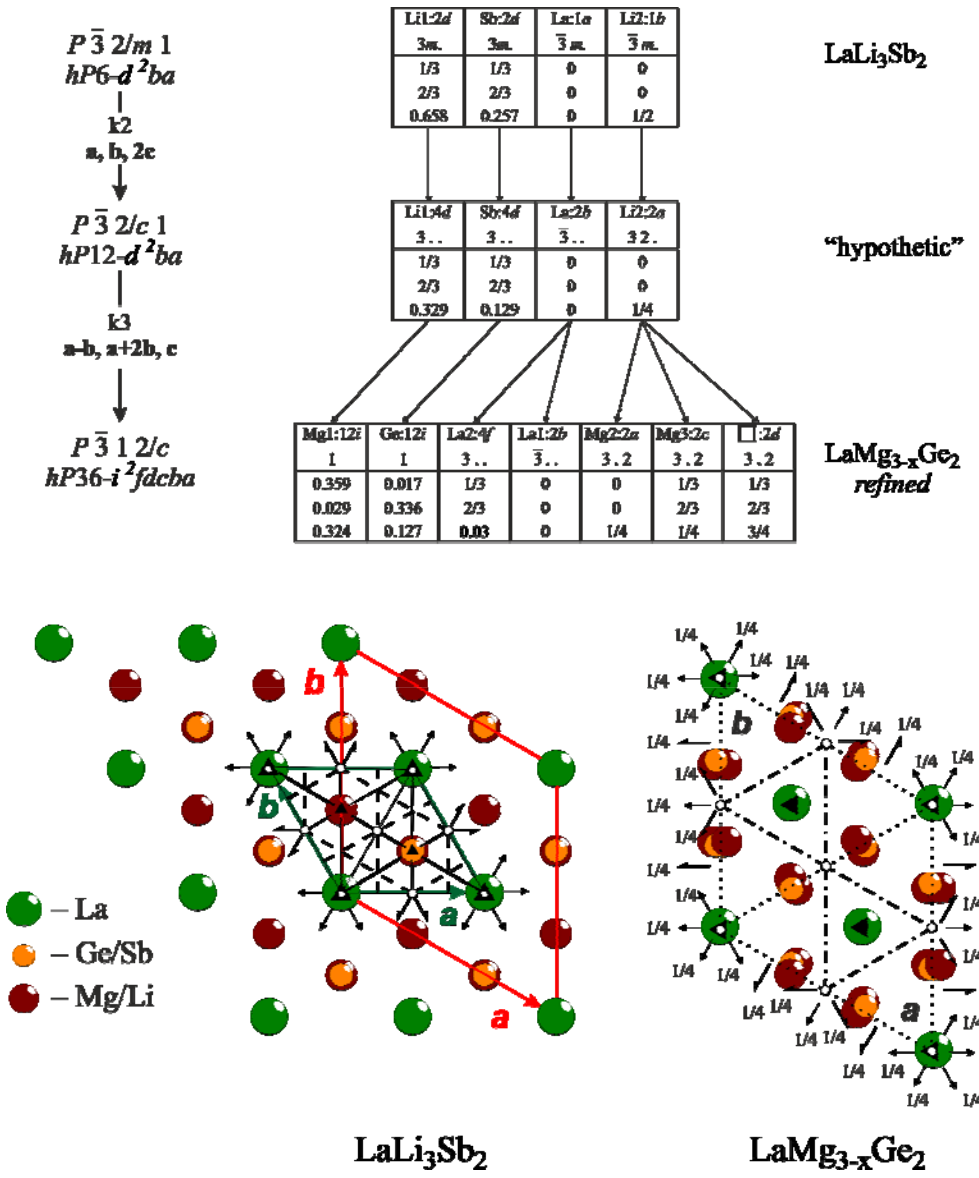
P 3̄ 2/m 1
hP6-d ²ba
k2
a, b, 2c
P 3̄ 2/c 1
hP12-d ²ba
k3
a-b, a+2b, c
P 3̄ 1 2/c
hP36-i ²fdcba
Li1:2d
Sb:2d
La:1a
Li2:1b
3m.
3m.
3̄ m.
3̄ m.
1/3
2/3
0.658
0.257
0
1/2
LaLi3Sb2
Li1:4d
Sb:4d
La:2b
Li2:2a
3..
3..
3̄..
32.
0.329
0.129
1/4
"hypothetic"
Mg1:12i
Ge:12i
La2:4f
La1:2b
Mg2:2a
Mg3:2c
□:2d
1
1
3..
3̄..
3.2
3.2
3.2
0.359
0.017
1/3
0.029
0.336
2/3
0.324
0.127
0.03
3/4
LaMg3-xGe2
refined
– La
– Ge/Sb
– Mg/Li
b
a
LaLi3Sb2
LaMg3-xGe2

Fig. 4.

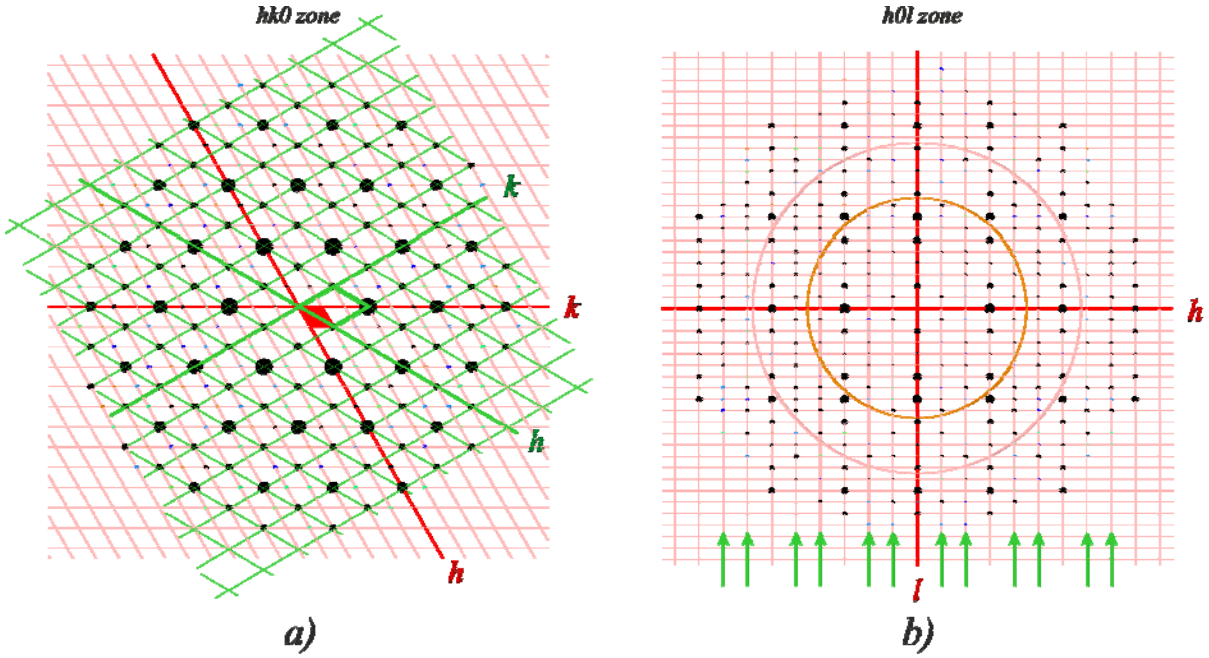

Fig. 5.

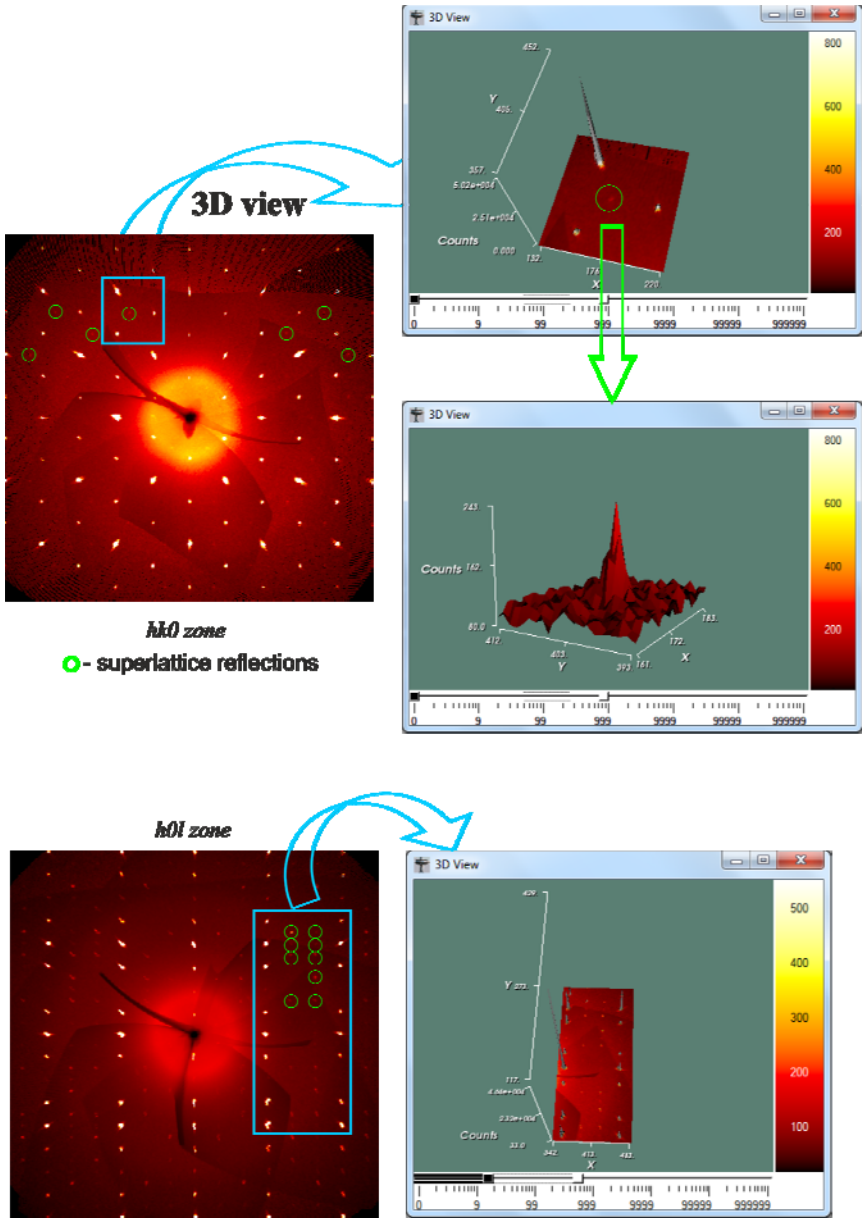
3D view
hk0 zone
- superlattice reflections
h0l zone
3D View
Counts

Fig. 6.

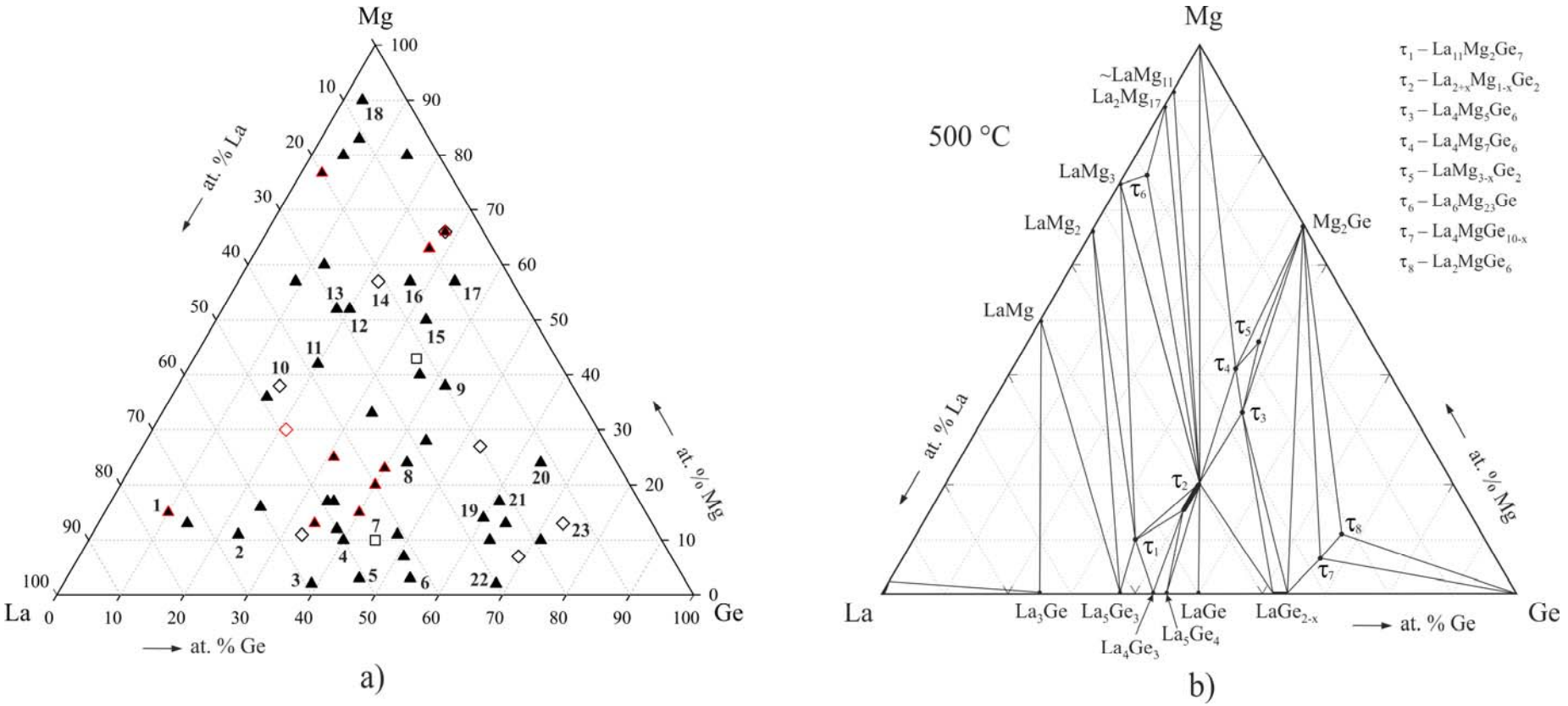
Mg
La
Ge
at. % La
at. % Mg
at. % Ge
a)
500 °C
~LaMg11
La2Mg17
LaMg3
LaMg2
LaMg
Mg2Ge
La3Ge
La5Ge3
La4Ge3
La5Ge4
LaGe
LaGe2-x
τ1 – La11Mg2Ge7
τ2 – La2+xMg1-xGe2
τ3 – La4Mg5Ge6
τ4 – La4Mg7Ge6
τ5 – LaMg3-xGe2
τ6 – La6Mg23Ge
τ7 – La4MgGe10-x
τ8 – La2MgGe6
b)

Fig.7.

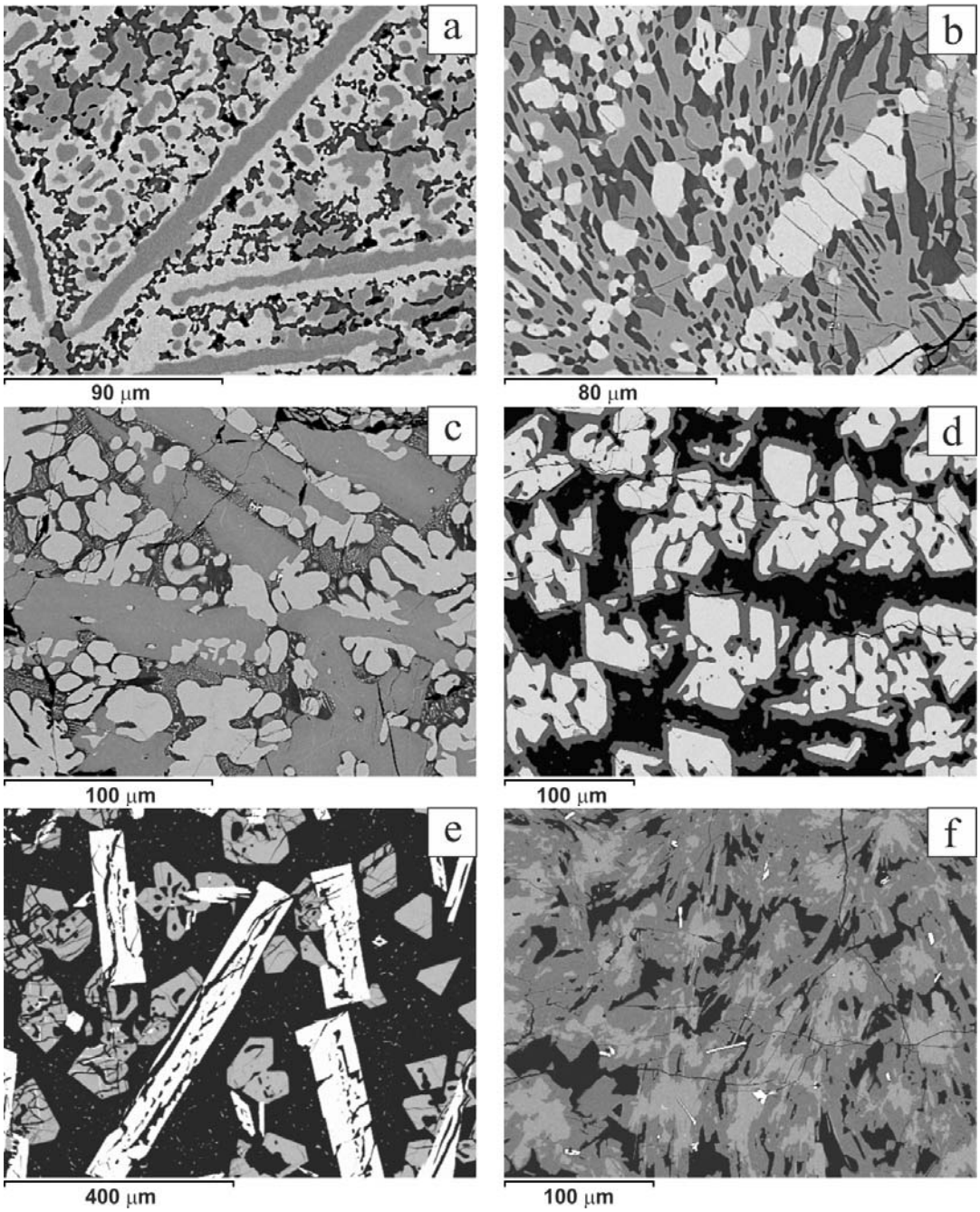

Fig. 8.